Journal of
Ceramic Science
and Technology

J. Ceram. Sci. Tech., **04** [03] 157-162 (2013)
DOI: 10.4416/JCST2013-00007
available online at: http://www.ceramic-science.com

PEG-Assisted Synthesis of Manganese Oxide Nanorods and Their Application as Electrode Material for Lithium-Ion Batteries

P. Ragupathy*[1], J. Sundaramurthy[2, 3], P. Suresh Kumar[2], V. Thavasi[2], S. Ramakrishna*[2, 3]

[1]Fuel Cell Section, Electrochemical Power Systems Division, Central Electrochemical Research Institute, Karaikudi 630 006, India
[2]NUS Nanoscience and Nanotechnology Initiative, National University of Singapore, Singapore 117576
[3]Center for Nanofibers and Nanotechnology, Mechanical Engineering, National University of Singapore, Singapore 117576

received March 17, 2013; received in revised form July 3, 2013; accepted September 4, 2013

Abstract

In this work, we report on large-scale synthesis of α-MnO_2 nanorods by the polyol route based on a simple redox reaction using an organic reducing agents potassium permanganate ($KMnO_4$) and polyethylene glycol (PEG). The as-synthesized amorphous MnO_2 is converted into crystalline form on annealing at temperature of 600 °C. The formation of MnO_2 nanorod-like morphology is confirmed with scanning electron microscopy complemented with high-resolution transmission electron microscopy. The nanorods measure about 50 – 200 nm in length and 50 nm in diameter. The electrochemical lithium intercalation and de-intercalation of nanorods are performed by means of galvanostatic charge-discharge cycling. The initial discharge capacity of nanorod α-MnO_2 is found to be about 214 mAh/g^{-1} with reasonably good rate capability.

Keywords: Manganese oxide, nanorods, lithium-ion batteries

I. Introduction

Nanotechnology has attracted intense research interest with regard to both its fundamental scientific significance and applications owing to the superior properties of nanotechnology components compared to corresponding bulk counterparts [1–4]. Building blocks on nanoscale such as nanotubes, nanowires, nanobelts, and nanorods have been identified for the next generation of nanodevices in the field of microelectronics and optoelectronics [5–7]. In recent years, it has been observed that nanomaterials play an important role in achieving high-energy and high-power-density rechargeable Li-ion batteries essential to meet future energy demand [8]. Most commercial Li-ion batteries use $LiCoO_2$ as electrode material on account of its superior electrochemical performance. However, the high cost and toxicity of Co prevent its successful commercialization [9, 10]. Against this background, research has been focused on lower-cost and environmentally friendly alternative materials such as manganese oxides. Manganese dioxide, MnO_2, is used in lithium secondary batteries [4, 11–14], supercapacitors [15–17] catalysts [18], biosensors [19, 20] and molecular adsorption [21] owing to its structural flexibility, excellent chemical and electrochemical stability, ecological and economical compatibility, and high abundance in nature. MnO_2 exists in different structural forms, that is α, β, γ and δ types, etc. depending upon the spatial arrangement of basic octahedral unit MnO_6 [11].

It is generally recognized that the kinetics of Li^+ intercalation/deintercalation are mainly controlled by the diffusion rate of Li^+ in the solid matrix. Nanostructured materials are expected to offer high specific capacity, and rate capability owing to their high aspect ratio and smaller diffusion path length for Li^+ transport compared to larger particles [8]. Particularly, the narrow diameter (or width) of 1-D nanostructures provides a much shorter Li^+ diffusion path to enhance the electrochemical properties. In order to develop high-performance nanoscale devices, it is essential to develop convenient synthesis strategies that yield new nanostructured materials with controlled morphologies, crystallographic forms and distinctive performance. Until now, the investigation of the 1-D nanostructured MnO_2 as electrode materials has remained limited, despite the fact that the shape and size of the material are generally known to influence the properties of the electrodes, and in turn their performance.

MnO_2 has often been prepared by means of (i) oxidation of Mn(II) with oxidant and (ii) reduction of MnO_4^- with reductant. As fruit of the intensive research activities devoted to this topic, many synthesis methods have been developed for 1-D manganese oxide. For instance, nanowires were obtained with electrochemical step-edge decoration and hydrothermal techniques [22–23]. Many researchers have prepared 1-D nanorods of MnO_2 by sol-

* Corresponding author: seeram@nus.edu.sg
ragupathyp@cecri.res.in

gel, hydrothermal and low-temperature liquid phase comproportion methods [20,24]. It is well known that MnO_2 transforms to Mn_2O_3 and Mn_3O_4 at higher temperatures, which is an obstacle for rechargeable Li-ion cells. It is always desirable to prepare dehydrated α-MnO_2 as cathode material for efficient intercalation and deintercalation of lithium in the tunnels. In this report, we demonstrate the large-scale preparation of MnO_2 nanorods based on the reduction of $KMnO_4$ with PEG at a high temperature.

II. Experimental

(1) Synthesis

All chemical reagents were purchased from Aldrich and used as-received. Typically, 3.16 g $KMnO_4$ was dissolved in 200 ml deionized water, and after complete dissolution, 20 ml PEG was added drop wise on vigorous stirring. The brownish-black colour precipitate confirmed completion of the reaction. The obtained precipitate was washed with deionized water several times and then rinsed with ethanol. The resultant amorphous precursor was annealed to 600 °C, which yielded the dehydrated and highly crystalline 1-D α-MnO_2 nanorods.

(2) Characterization

Powder X-ray diffraction (XRD) patterns of the synthesized products were recorded using a Philips XRD 'X' PERT PRO diffractometer with CuKα as a source. The morphology and structural properties of the as-synthesized products were further investigated by means of field emission scanning electron microscopy (FESEM, JEOL, JSM 6700F) and high-resolution transmission electron microscopy (HRTEM, Tecnai). A Sartorius balance, model CP22D-OCE, with 10 μg sensitivity was used to weigh the electrodes and materials.

(3) Electrode preparation and electrochemical characterization

The electrochemical performance of the cathodes was evaluated with CR2032 coin cells (cell components from Hohsen Corp., Japan) fabricated with metallic lithium anode and 1 M $LiPF_6$ in ethylene carbonate (EC) and diethyl carbonate (DEC) electrolyte (from EM Industries Inc.). The cathodes were fabricated by mixing 75 wt% active material, 20 wt% binder of conducting carbon and 5 wt% poly-tetrafluoroethylene (PTFE) with a few drops of isopropyl alcohol, then rolling the mixture into thin sheets, which were then cut into circular electrodes of the size 0.64 cm^{-2}. The cathodes and cell components were dried at 110 °C overnight in a vacuum. Cells were assembled in an argon-filled glove box. A Celgard microporous polypropylene film was used as the inter-electrode separator. An Arbin battery tester was used for galvanostatic charge-discharge cycling.

III. Results and Discussion

The crystalline phase and purity of the sample were determined by means of powder XRD analysis. Fig. 1 shows the powder XRD patterns of as-synthesized MnO_2 and annealed MnO_2. The sample synthesized at room temperature was amorphous in nature as shown in Fig. 1a. Upon heat treatment at 600 °C, it formed highly crystalline MnO_2 (Fig. 1b). All the diffraction lines were indexed on the basis of the tetragonal phase (space group I4/m) of α-MnO_2 (JCPDS 44 – 0141). The morphology of the obtained α-MnO_2 is shown in the FESEM images in Fig. 2. Amorphous oxides exhibited highly clustered granules of varying size between 30 and 50 nm as seen in Fig. 2a. The formation of nanorods of the α-MnO_2 was clearly seen upon sintering of the as-synthesized MnO_2 at 600 °C. A magnified SEM image indicates that the individual nanorods have a size of about 50 – 200 nm in length and 50 nm in diameter (Fig. 2b).

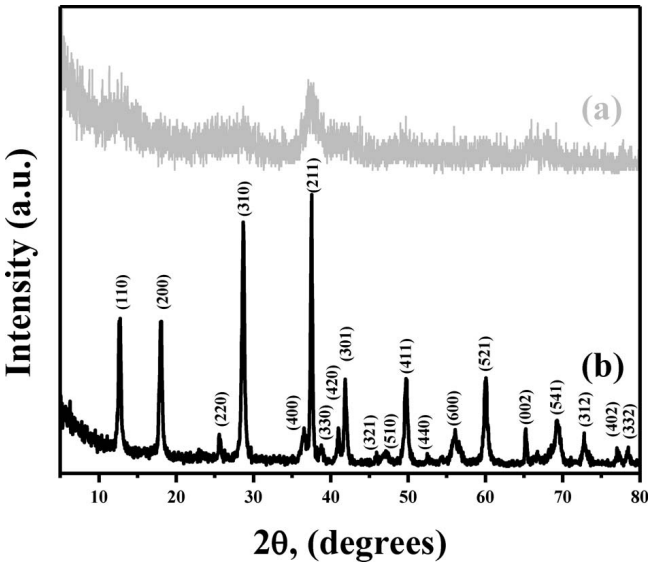

Fig. 1: Powder XRD diffraction patterns of (a) as-prepared MnO_2 and (b) annealed α-MnO_2 at 600 °C.

Fig. 3a shows the typical TEM image of α-MnO_2 nanorods formation using the present approach and is consistent with earlier observations. EDAX shown as an inset in Fig. 3b indicates the presence of Mn, O and a trace amount of K in the sample. The recorded FFT of α-MnO_2 confirms the crystalline nature of the individual rods as seen in Fig. 3c. The clear lattice fringes are evident from HRTEM image as seen in Fig. 3d. The interplanar spacing between two fringes is 0.69 nm, corresponding to (110) plane as observed in the XRD pattern.

In order to assess the electrochemical performance of nanorods α-MnO_2, the fabricated electrodes were galvanostatically cycled between 1.5 and 4.3 V vs. Li^+/Li. The charge-discharge curves of the α-MnO_2 electrode recorded at 23.6 mAg^{-1} are shown in Fig. 4. These two-stage processes of lithium insertion and extraction of the α-MnO_2 material were clearly explained in the literature [11]. First step of lithium insertion was attributed to a single-phase process in which lithium is inserted into an α-MnO_2 framework to form $Li_{0.5}MnO_2$. The second stage of lithium insertion occurred in Jahn-Teller-distorted Mn ions, when the average manganese oxidation state reaches 3.5 in the electrode materials. In the present study, α-MnO_2 nanorod electrodes exhibited the initial discharge capacity of about 214 mAh/g^{-1}, which corresponds to 0.70 Li, and maximum Li insertions occurred at higher voltage (≥ 2 V). Recently, Kijima *et al* [25]. have reported the discharge capacity of 230 mAh/g^{-1} for α-MnO_2 at a lower current density of 10 mAg^{-1}. The nanorods of α-MnO_2 with the

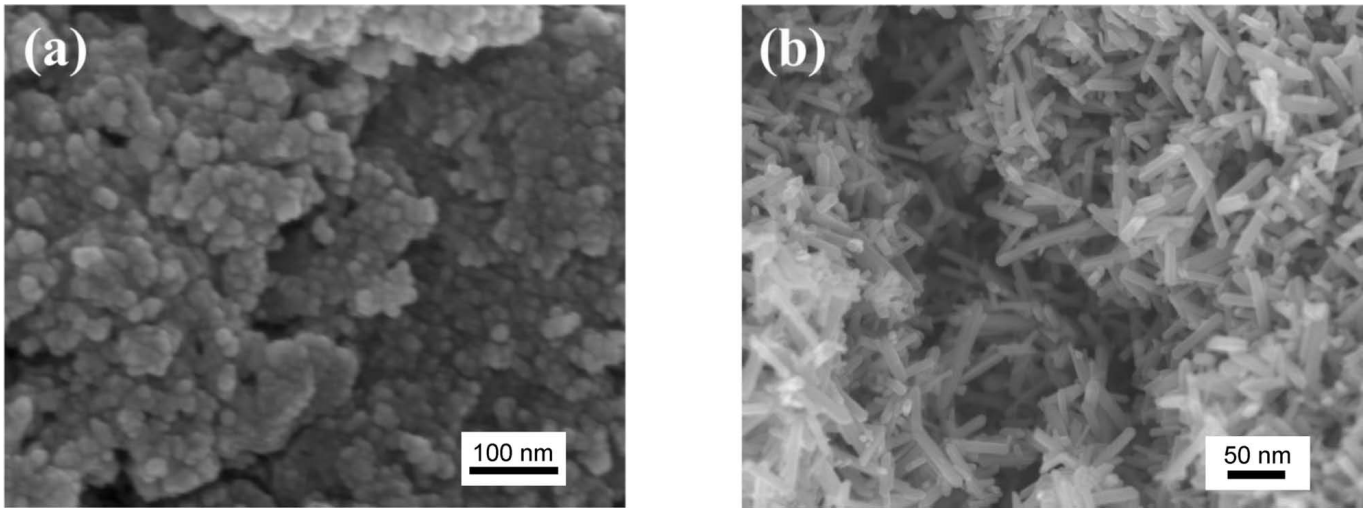

Fig. 2: SEM images of (a) as-prepared amorphous MnO_2 nanoparticles and (b) crystalline α-MnO_2 nanorods after annealing at 600 °C.

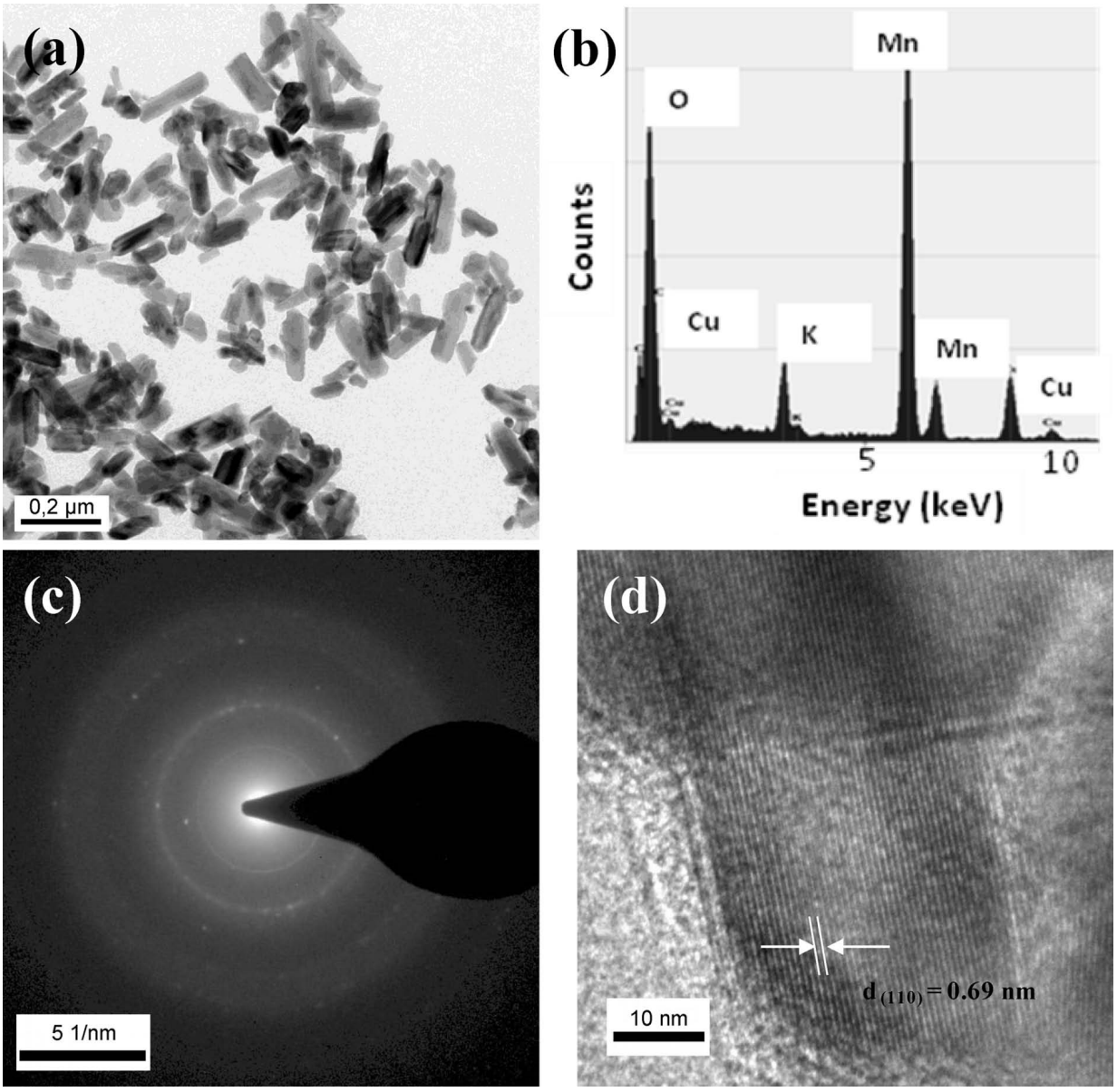

Fig. 3: (a) TEM image of α-MnO_2 nanorods, (b) EDAX pattern of nanorods, (c) SAED ring pattern and (d) HRTEM image of single α-MnO_2 nanorod.

present method offers the discharge capacity of 214 mAg^{-1} even at a high current density of 23.6 mAg^{-1}. The value is comparable with the reported α-MnO_2 nanofibres. Moreover, the obtained discharge capacity of nanorods is much higher than that of bulk materials. It is well documented that γ-MnO_2 demonstrates better electrochemical performance than α-and β-MnO_2 as cathode materials in batteries. However; the discharge capacity of the obtained α-MnO_2 nanorods in the present work is even higher than that of the γ-MnO_2 commercial powders. Hence, the as-synthesized 1-D nanostructured α-MnO_2 shows an enhanced performance. To check the rate capability of the α-MnO_2, the electrodes were subjected to charge discharge cycling at different current densities. The specific capacity of nanorod electrodes against different C-rates is shown in Fig. 5. On increasing the C-rate from 0.1 C-rate to 0.2 C-rate, the initial capacity was reduced from 170 to 150 mAh/g^{-1} which is approximately 79 % and 70 % of the capacity observed at 0.1 C-rate. Similar behaviour was observed earlier with other electrode materials [26, 27]. Cycle-life studies were performed with α-MnO_2 electrodes at 0.1 C-rate. The specific capacity of nanorods α-MnO_2 was found to be 67 mAh/g^{-1} after 25 cycles, which corresponds to 31 % of the initial capacity as shown in Fig. 6. Upon repeated cycling, the capacity reduces further to 40 mAh/g^{-1} after 50 cycles. This capacity loss is attributed to the fraction of lithium ions inserted during the initial discharge becoming locked within the tunnels of MnO_2 for structural stabilization, inherent structural properties of MnO_2 and structural change from α-MnO_2 framework to a defect rock salt structure. However, the capacity retention can be improved by modifying the surface with ZnO and TiO_2 coating, which is currently being studied with the aim of stabilizing capacity values and rate capability.

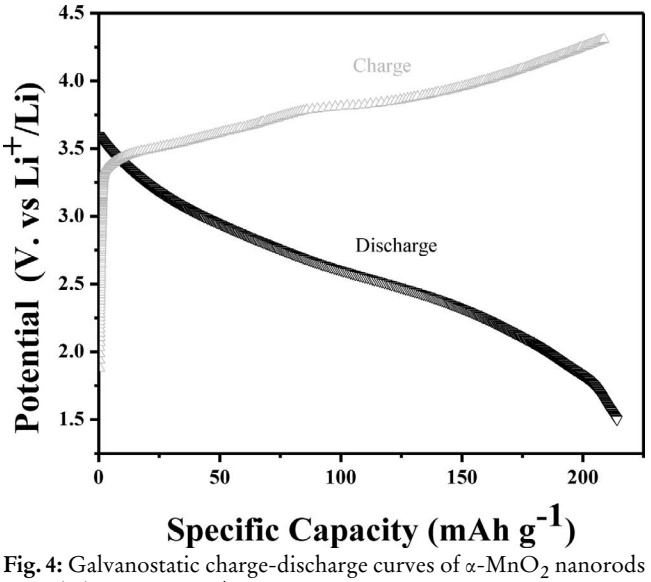

Fig. 4: Galvanostatic charge-discharge curves of α-MnO_2 nanorods recorded at 23.6 mAg^{-1}.

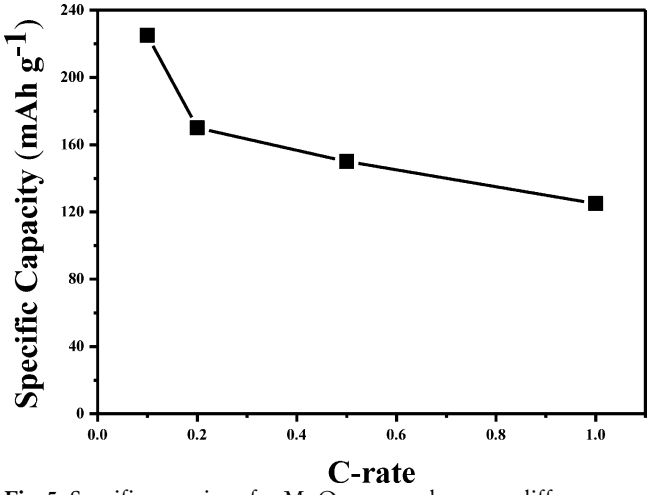

Fig. 5: Specific capacity of α-MnO_2 nanorods versus different current densities.

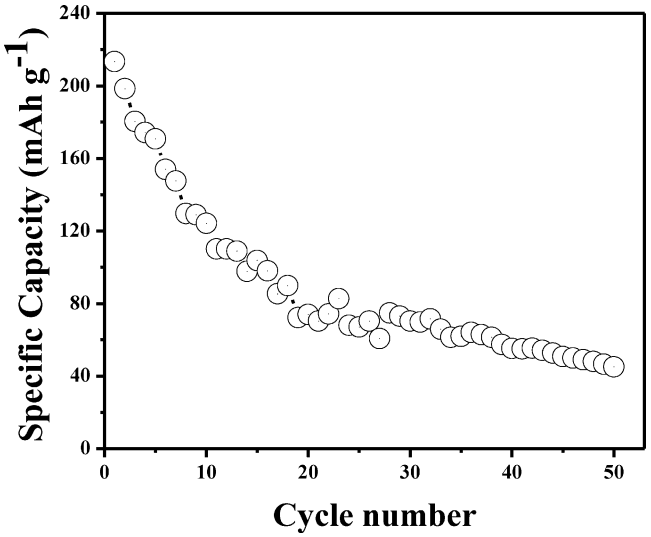

Fig. 6: Discharge capacity of α-MnO_2 nanorods versus cycle number recorded in ambient conditions.

IV. Conclusions

The large-scale synthesis of MnO_2 nanorods was successfully demonstrated based on the simple redox reaction of $KMnO_4$ using PEG. Interestingly upon sintering at 600 °C, the amorphous MnO_2 was converted into α-phase without undergoing conversion into Mn_2O_3 at higher temperatures. Electrochemical studies revealed that the initial discharge capacity of nanorod α-MnO_2 was about 214 mAh/g^{-1} at 0.1 C-rate. These results indicate the potential large-scale synthesis of MnO_2 with nanorod-like morphology as an efficient electrode material for Li-ion batteries.

References

1 Nalwa, H.S.: Handbook of nanostructured materials and nanotechnology, Academic Press: New York, 2000.

2 Burda, C., Chen, X., Narayanan, R., El-Sayed, M.A.: Chemistry and properties of nanocrystals of different shapes, *Chem. Rev.*, **105**, 1025 – 1102, (2005).

3 Bell, A.T.: The impact of nanoscience on heterogeneous catalysis, *Science*, **299**, 1688 – 1691, (2003).

4 Tarascon, J.-M., Armand, M.: Issues and challenges facing rechargeable lithium ion batteries, *Nature*, **414**, 359 – 367, (2001).

5 Xia, Y., Yang, P., Sun, Y., Wu, Y., Mayers, B., Gates, B., Yin, Y., Kim, F., Yan, H.: One-dimensional Nanostructures: Synthesis, characterization, and applications, *Adv. Mater*., **15**, 353 – 389, (2003).

6 Wang, J., Wang, X., Peng, Q., Li, Y.: Synthesis and characterization of bismuth single-crystalline nanowires and nanospheres, *Inorg. Chem*., **43**, 7552 – 7556, (2004).

7 Duan, X., Huang, Y., Cui, Y., Wang, J., Lieber, C.M.: Indium phosphide nanowires as building blocks for nanoscale electronic and optoelectronic devices, *Nature*, **409,** 66 – 68, (2001).

8 Bruce, P.G., Scrosati, B., Tarascon, J.M.: Nanomaterials for rechargeable lithium batteries, *Angew. Chem. Int. Ed*., **47**, 2930 – 2946, (2008).

9 Sun, Y- K., Yoon, C.S., Kim, C.K., Youn, S.G., Lee, Y-S., Yoshio, M., Oh, I-H.: Degradation mechanism of spinel $LiAl_{0.2}Mn_{1.8}O_4$ cathode materials on high temperature cycling, *J. Mater. Chem*., **11**, 2519 – 2522, (2001).

10 Yan, H., Huang, X., Chen, L.: Microwave synthesis of $LiMn_2O_4$ cathode material, *J. Power Sources*, **81 – 82**, 647 – 650, (1999).

11 Thackeray, M.M.: Manganese oxides for lithium batteries, *Prog. Solid State Chem.*, **25,** 1 – 71, (1997).

12 Cheng, F., Zhao, J., Song, W., Li, C., Ma, H., Chen, J., Shen, P.: Facile controlled synthesis of MnO_2 nanostructures of novel shapes and their application in batteries, *Inorg. Chem*., **45,** 2038 – 2044, (2006).

13 Zhang, R., Yu, X., Nam, K.W., Ling, C., Arthur, T.S., Song, W., Knapp, A.M., Ehrlich, S.N., Yang, X.Q., Matsui, M.: α-MnO_2 as a cathode material for rechargeable Mg batteries, *Electrochem. Comm*., **23,** 110 – 113, (2012).

14 Lei, Z., Shi, F., Lu, L.: Incorporation of MnO_2-coated carbon nanotubes between graphene sheets as supercapacitor electrode, *ACS Appl. Mater. Interfaces*, **4**, 1058 – 1064, (2012).

15 Brousse, T., Toupin, M., Dugas, R., Athouel, L., Crosnier, O., Belanger, D.: Crystalline MnO_2 as possible alternatives to amorphous compounds in electrochemical supercapacitors, *J. Electrochem. Soc.,* **153,** A2171 – A2180, (2006).

16 Devaraj, S., Munichandraiah, N.: Electrochemical supercapacitor studies of nanostructured α-MnO_2 synthesized by microemulsion method and the effect of annealing, *J. Electrochem. Soc*., **154**, A80, (2007).

17 Ragupathy, P., Vasan, H.N., Munichandraiah, N.: Synthesis and characterization of nano-MnO_2 for electrochemical supercapacitor studies, *J. Electrochem. Soc*., **155**, A34 – A40, (2008).

18 Espinal, L., Suib, S.L., Rusling, J.F.: Electrochemical catalysis of styrene epoxidation with films of MnO_2 nanoparticles and H_2O_2, *J. Am. Chem. Soc.,* **126,** 7676 – 7680, (2004).

19 Luo, X.L., Xu, J.J., Zhao, W., Chen, H.Y.: A novel glucose ENFET based on the special reactivity of MnO_2 nanoparticles, *Biosens. Bioelectron.*, **19,** 1295 – 1300, (2004).

20 Yu, J., Zhao, T., Zeng, B.: Mesoporous MnO_2 as enzyme immobilization host for amperometric glucose biosensor construction, *Electrochem. Comm*., **10**, 1318 – 1321, (2008).

21 Chitrakar, R., Kanoh, H., Kim, Y.S., Miyai Y., Ooi, K.: Synthesis of layered-type hydrous manganese oxides from monoclinic-type $LiMnO_2$, *J. Solid State Chem*., **160**, 69 – 76, (2001).

22 Wang, X., Li, Y.: Selected-control hydrothermal synthesis of α-and β-MnO_2 Single Crystal Nanowires, *J. Am. Chem. Soc.,* **124**, 2880 – 2881, (2002).

23 Liu, Y., Zhang, M., Zhang, J., Qian, Y.: A simple method of fabricating large-area α-MnO_2 nanowires and nanorods, *J. Solid State Chem*., **179**, 1757 – 1761, (2006).

24 Xu, J.J., Luo, X.L., Du Y., Chen, H.Y.: Application of MnO_2 nanoparticles as an eliminator of ascorbate interference to amperometric glucose biosensors, *Electrochem. Comm*., **6**, 1169 – 1173, (2004).

25 Kijima, N., Takahashi, Y., Akimoto, J., Awaka, J.: Lithium ion insertion and extraction reactions with Hollandite-type manganese dioxide free from any stabilizing cations in its tunnel cavity, *J. Solid State Chem.,* **178**, 2741 – 2750, (2005).

26 Suresh, P., Rodrigues, S., Shukla, A.K., Shivashankar S.A., Munichandraiah, N.: Synthesis of $LiCo_{1-x}Ni_xO_2$ from a low temperature solution combustion route and characterization, *J. Power Sources*, **112**, 665 – 670, (2002).

27 Suresh, P., Rodrigues, S., Shukla, A.K., Vasan H.N., Munichandraiah, N.: Synthesis of $LiCo_{1-x}Mn_xO_2$ from a low-temperature route and characterization as cathode materials in Li-ion cells, *Solid State Ionics*, **176**, 281, (2005).